New Journal of Physics
The open access journal at the forefront of physics

Deutsche Physikalische Gesellschaft DPG
IOP Institute of Physics

Published in partnership with: Deutsche Physikalische Gesellschaft and the Institute of Physics

OPEN ACCESS

RECEIVED
25 August 2016

REVISED
22 October 2016

ACCEPTED FOR PUBLICATION
8 November 2016

PUBLISHED
24 November 2016

PAPER

Mechanism of self-propulsion in 3D-printed active granular particles

N Koumakis[1,2,5], A Gnoli[3,4], C Maggi[4], A Puglisi[3,4] and R Di Leonardo[1,4]

[1] NANOTEC-CNR, Institute of Nanotechnology, Soft and Living Matter Laboratory, Piazzale A. Moro 2, I-00185, Roma, Italy
[2] School of Physics and Astronomy, University of Edinburgh, Edinburgh, EH9 3JZ, UK
[3] Istituto dei Sistemi Complessi—Consiglio Nazionale delle Ricerche, Rome, Italy
[4] Dipartimento di Fisica, Università di Roma Sapienza, I-00185, Rome, Italy
[5] Author to whom any correspondence should be addressed.

E-mail: nkoumakis81@googlemail.com

Keywords: active matter, granular propulsion, 3D printing

Supplementary material for this article is available online

Abstract

Active granular particles can harness unbiased mechanical vibrations in the environment to generate directed motion. We provide a theoretical framework that connects the geometrical shape of a three dimensional object to its self-propulsion characteristics over a vertically vibrated plate. We find that a maximally efficient propulsion is achieved for structures having tilted flexible legs forming a characteristic angle with the vertical. Our predictions are verified by experimental observations on a class of 3D printed structures with smoothly varying geometrical features.

Active matter refers to a wide class of many-particle systems that can locally convert environmental energy into directed motion [1–4]. The collective behaviour of active systems displays many similarities across both the micro and macro scale and the biological and artificial domain. On the other hand, the physical mechanisms leading to self-propulsion can be enormously different across scales and domains. While viscous forces dominate at the micron scale, self-propulsion at the macroscopic scale is based on inertia, gravity and dry friction [5]. In macroscopic artificial systems, self-propulsion is obtained in many different ways with a varying degree of complexity. Minimal strategies are however particularly interesting in the context of active matter physics since they can be replicated in very large numbers opening the way to the study of collective phenomena in artificial systems. One of the simplest available strategies is that of rectifying mechanical vibrations using simple structures with asymmetric features. The source of vibration can be embedded in the particle itself, like in the so called 'bristlebots' [6, 20], or it can be externally applied to the particles, like in the case of vibrated granulars. Examples in this last category include rods [7–9] or discs [10–12] having linear dimensions in the range of mm, and fabricated with spatial asymmetries, in order to produce a persistent motion over a vertically vibrating plate [7–9, 13–16]. In [10], polar discs have been designed by adding two artificial 'legs' below each disk and manufactured individually by hand. Collective ordered phases were observed, and their properties further studied in [11, 12, 17]. Single-particle studies [18, 19] as well as analyses of collective properties [10, 11], have demonstrated the strong analogy between such systems and other examples of active matter. Despite the strong interest in these kind of systems, even outside of the scientific scope (the bristlebot is a very popular toy too), the physical mechanism leading to propulsion is still poorly understood in quantitative terms.

In this work we combine experiments, theory and simulations to describe quantitatively how propulsion arises in a simple model for an active granular particle having two tilted flexible legs and bouncing over a vertically vibrated plate. We use 3D printing to fabricate a one-parameter family of shapes having inclined legs and measure several properties of the single-particle motion restricted to a lane or freely moving on a plane. A theoretical model, describing propulsion as a sequence of impacts with friction, highlights the importance of flexibility in the legs and predicts the existence of an optimal legs' inclination angle which maximizes the propulsion speed. These predictions are quantitatively verified with experimental observations.

We consider a minimal model for an active granular particle that is composed of three rigid parts (see figure 1-bottom): (i) a massive top whose centre of mass, total mass and moment of inertia are indicated

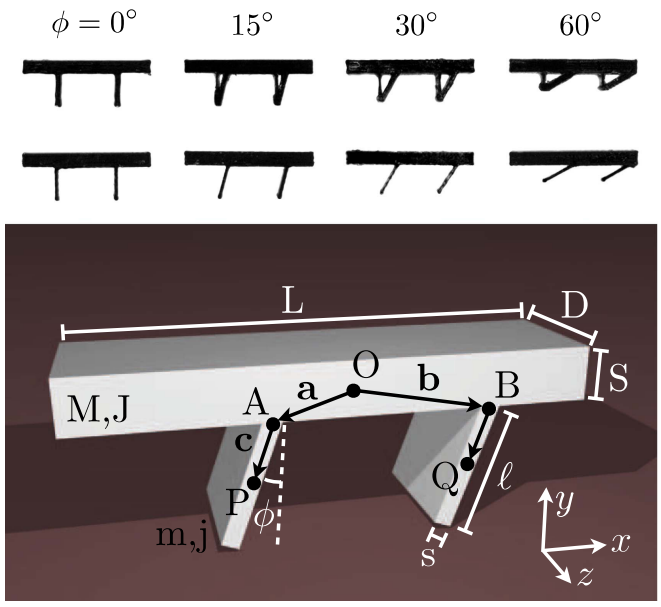

Figure 1. (Top panel) Photo of the 3D printed walkers used in the experiment, structures in top row have connected (rigid) legs and structures in bottom row have free (flexible) legs. (Bottom panel) Scheme of the idealized walker considered in the theory.

respectively by O, M, J; (ii) two legs having centres in P and Q and the smaller values m and j for the mass and inertia moment. The legs are anchored to the top at points A and B forming an angle $\pm$ with respect to the top normal. As opposed to bristlebot models, where structures are always in contact with the surface [6, 20], in our model of active granular particles forward propulsion arises from a rapid sequence of collisions where the vertical momentum of the vibrating surface is partially transferred to the horizontal direction. We assume that impacts can only occur at one of the two contact points and never simultaneously on both. Let us first consider the case of a totally rigid structure free falling on a static substrate with vertical speed $-v_y^0$. We assume that the legs have a negligible mass compared to the top so that the entire structure has centre of mass in O and a total mass and moment of inertia given by M and J. We assume that the impact is instantaneous meaning that only impulsive forces need to be considered and that the structure configuration can be kept fixed during the entire duration of the collision. Assuming a collision occurs at the back leg and calling f the impulsive reaction force, the dynamical equations read:

$$M\dot{v}_O = f, \quad J\dot{\omega} = d \times f, \tag{1}$$

where $d = a + 2c$ is the vector position of the back leg contact point relative to the centre of mass O. Integrating (1) between time $t = 0$ (impact) and a generic time t during collision we get

$$M\Delta v_O = F, \; J\Delta\omega = d \times F, \tag{2}$$

where $F = \int_0^t f(t')dt'$ is the impulse of the reaction force. Calling v_c the speed of the contact point we can write the corresponding acceleration $\dot{v}_c = \dot{v}_O + \dot{\omega} \times d$. In the last equation we only kept terms involving the velocities derivatives by dropping out terms scaling as velocities squared that are negligible during impact. Integrating the last equation and substituting (2) we get

$$\Delta v^c = \mathcal{M} \cdot F, \tag{3}$$

with $\mathcal{M}$ a symmetric tensor having the physical dimensions of an inverse mass and whose structure is solely specified by the prescribed geometry:

$$\mathcal{M} = \frac{1}{M}\mathbb{1} + \frac{d^2}{J}[\mathbb{1} - \hat{d}\hat{d}]. \tag{4}$$

The free falling body will touch the surface with a zero horizontal speed of the contact point. We can use (3) to answer the questions: what is the sign of the static friction force required to prevent sliding and what is the minimum required static friction coefficient? To this aim we impose $\Delta v_x^c = 0$ in (3) and solve for F_x finding $F_x = -(H_{xy}/H_{xx})F_y$. Since F_y and H_{xx} are always positive, the static friction force that would be required to prevent sliding points in the direction given by $s = -\mathrm{sgn}(H_{xy})$ while the static friction coefficient has to satisfy $\mu_s > |H_{xy}|/|H_{xx}|$. We will assume for the moment that the static friction coefficient is never high enough and that the contact point will therefore start sliding along the x axis in the direction given by $-s$ while a dynamic friction force will act in the opposite direction σ. Assuming Coulomb friction, the total reaction force from the substrate

will then be $\mathbf{f} = (\mu f_y, f_y)$ with μ the dynamic friction coefficient. Following [21] we can now calculate the total impulse that is transferred to the structure during impact in two steps. First, we solve the y component of (3) to get the total vertical impulse $F_y^\star$ that the substrate transfers to the structure up to the point of maximum compression when the vertical speed of the contact point vanishes - $v_y^0 + \Delta v_y^c = 0$ which implies

$$F_y^\star = \frac{v_y^0}{\mu |H_{yx} + H_{yy}|} = \frac{v_y^0}{H_{yy} - \mu |H_{xy}|}. \tag{5}$$

We then assume a Poisson restitution law and get the final vertical impulse, after decompression and detachment of contact point as $F_y^{tot} = (1 + e)F_y^\star$ with e the restitution coefficient. The total impulse transferred in the horizontal direction is finally obtained as

$$F_x^{tot} = \mu |F_y^{tot}| = \frac{\mu (1 + e) v_y^0}{H_{yy} - \mu |H_{xy}|}, \tag{6}$$

where from (4) we get $H_{xy} = -d_x d_y / J$ and $H_{yy} = 1/M + d_y^2/J$. The corresponding amount of transferred angular momentum will be:

$$J\Delta\omega = d \times F^{tot} = \frac{(d_x - \mu |d_y|)(1 + e) v_y^0}{H_{yy} - \mu |H_{xy}|} \hat{z}. \tag{7}$$

The angular momentum change has the leading, zero order term in friction $d_x v_y^0 / H_{yy}$ so that front collisions transfer positive angular momentum along z while back collisions transfer negative momentum. The total horizontal component of transferred linear momentum is positive ($s > 0$) when a collision occurs on the back leg and negative ($s < 0$) for a collision on the front leg. Therefore a net propulsion will be generated when this two contributions are unbalanced. One possibility would be to change the physical characteristics of the contact points, like for example using two different materials having different friction or restitution coefficients [10]. While, if we want to build our structure from the same material, the only option would be to have an asymmetric structure having unequal leg lengths and two different values of d_x, and hence H_{xy} for the two contact points. In this case, the difference in F_x^{tot} will only be second order in friction, while the leading first order term in (6) will be equal and opposite for the two contact points. However, the net transfer of angular momentum has to vanish for stable motion and if, for example, we make d_x shorter for the back leg, a larger number of collisions are expected to occur on the back to compensate for the larger amount of momentum transferred in a front collision, thus resulting in a net positive propulsion [7]. In all above strategies, back and front collisions always compete by correspondingly accelerating and decelerating the object. The situation changes completely when we introduce flexible legs. The rigid case assumes that the joints A and B, connecting the two legs to the massive top of the structure, have an infinite stiffness that is always capable of counterbalancing impulsive torques, even for the infinitesimal deformations that occur during the short collision time. We now consider the case of flexible joints with a finite stiffness so that the restoring torques will always be negligible on the dynamical scale of impulsive torques and we can treat the joints as torque free. Slow motion movies of bouncing structures from a lateral viewpoint show that during impact the structures do not deform neither rotate appreciably. Therefore, as in the rigid case, we assume a constant geometry during impact (constant $\hat{a}$, $\hat{b}$, and $\hat{c}$) and obtain the total linear momentum transferred in a vertical impact on the back leg as:

$$M\dot{v}_O = g, \quad J\dot{\omega} = a \times g, \tag{8}$$

$$m\dot{v}_P = f + g, \quad j\dot{\omega} = c \times (f + g), \tag{9}$$

where g is the gravity force and ω is the angular speed of the leg around its centre of mass P that moves with a linear speed

$$v_P = v_O + \omega \times a + \omega \times c. \tag{10}$$

The velocity of the contact point is now given by:

$$v_C = v_O + \omega \times a + 2\omega \times c. \tag{11}$$

By differentiating (10) and (11) (again discarding terms involving velocities squared) and substituting equations (8) and (9) we obtain again a linear expression like (3) connecting Δv_C to the total impulse of the reaction force F where the tensor $\mathcal{K}$ now takes the form:

$$\mathcal{K} = \left[\frac{\mathbf{1}}{M} + \frac{a^2}{J}\mathbf{1} + \frac{2c^2}{j}\mathbf{1}\right] \cdot \left[\frac{\mathbf{1}}{m} - \frac{c^2}{j}\mathbf{1}\right] \cdot \left[\left(\frac{\mathbf{1}}{M} + \frac{1}{m}\right) + \frac{a^2}{J}\mathbf{1} + \frac{c^2}{j}\mathbf{1}\right]^{-1} + \frac{2c^2}{j}\mathbf{1} \tag{12}$$

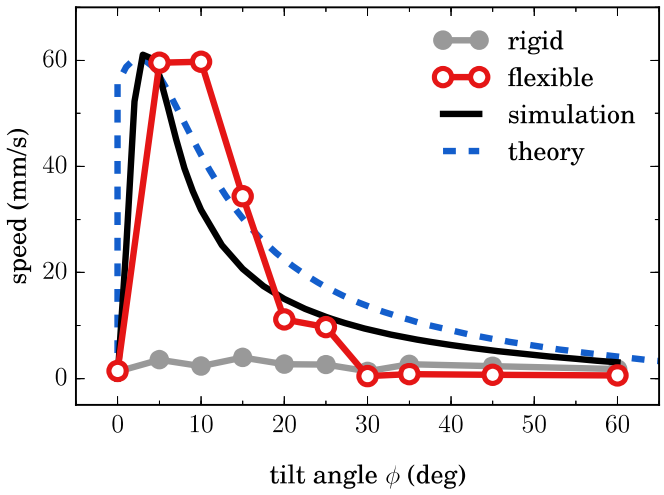

Figure 2. Average speed as a function of the leg tilt angle in experiments, theory and simulations. A clear peak at around f » 10 is found for flexible structures.

with = ââ and = ĉĉ. The analogous tensor for collisions occurring at the front leg is obtained by replacing with = b̂b̂. As for the rigid case, the total linear momentum transferred in a vertical impact on the back leg will be given by (6). The sign σ of F_x^{tot} can be easily obtained in the limit of m M, and hence j ml²/3 J ML²/3. In this approximation we get, for collisions on both the back or front leg, H_{xy} » - (3/m)cos f sin f and hence s > 0. As opposed to the rigid case the sign σ of the friction force is always positive and we expect to see a net positive momentum transfer on a vibrating plate that is first order in friction even in the symmetric case. Unfortunately, replacing the leading 1/m order of in (6) leads to divergences at a specific angle depending on μ and higher orders need to be included. However, once all parameters are specified, can be easily evaluated numerically. In order to compare our theory with experiments we need to make a prediction for the average propulsion speed that the structure will acquire on a vibrating plate. A reasonable estimate is obtained by assuming that the structure collides with the substrate with a speed that also possesses an horizontal, unknown component v_x^0. We then calculate the net horizontal momentum that is transferred during impact as a function of v_x^0. The stationary value of the propulsion speed is then obtained as the value of v_x^0 for which the transferred horizontal momentum vanishes. When a horizontal speed component is present we have to split the collision in three phases. During the first phase s < 0 and the friction forces bring the horizontal contact point speed to zero. In the second phase s > 0 and reaction forces bring the vertical component of the contact point speed to zero. In the last phase a fraction *e* of the vertical impulse transferred in the first two phases is restituted. In the first phase we have from (3) $\Delta v_x^1 = - v_x^0$, i.e.

$$F_y^1 = - \frac{v_x^0}{- mH_{xx} + H_{xy}}, \quad \Delta v_y^1 = (- mH_{xy} + H_{yy})F_y^1. \tag{13}$$

In the second phase $\Delta v_y^1 + \Delta v_y^2 = - v_y^0$ which gives

$$F_y^2 = \frac{1}{mH_{xy} + H_{yy}}(- \Delta v_y^1 - v_y^0) \tag{14}$$

and finally $F_y^3 = e(F_y^1 + F_y^2)$. The total transferred horizontal momentum will then be: $F_x^{tot} = - mF_y^1 + mF_y^2 + mF_y^3$. Solving $F_x^{tot} = 0$ for v_x^0 we get for the stationary speed:

$$v_x^0 = \frac{v_y^0(1 + e)}{2}\frac{H_{xy} - mH_{xx}}{H_{yy} - emH_{xy}}. \tag{15}$$

Equation (15) predicts a stationary value for the speed that is given by the product of two factors: the first one is the typical vertical relative speed at collision v_y^0, that is mainly controlled by (and of the same order of) the speed of the vibrating plate, the second factor depends on the mechanical properties of contacts (e, m) and the geometry of the structure through . Interestingly the geometric factor displays a maximum for small tilt angle f as shown in figure 2. The same non-monotonic behaviour is found in numerical simulations, which are also reported in figure 2 and described in more detail further in the text. The shape of speed versus f curve is very robust and displays a maximum that is always below 10° in a wide range of realistic values for *e* and μ. It is also interesting to note that the actual geometry of the objects only determines the propulsion speed through a ratio of different matrix components that does not depend on the total mass of the object nor on its scale. Within our 2D restricted theoretical analysis, the width *D* of the object only affects the total mass and thus has no effect

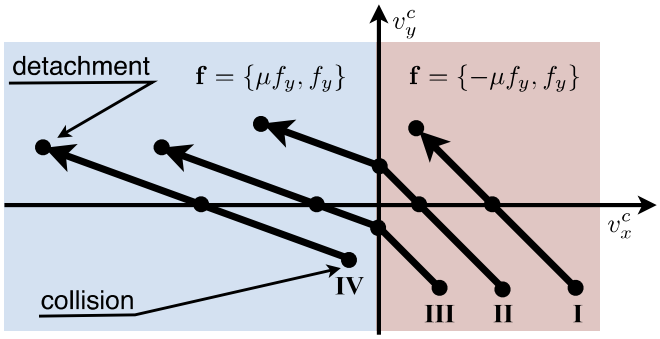

Figure 3. Collision types: (I) the horizontal contact point speed v_x^c is positive throughout the collision, (II) v_x^c is positive at maximum compression $v_y^c = 0$ but becomes negative during restitution, (III) v_x^c becomes negative before maximum compression, (IV) v_x^c is always negative.

on the propulsion speed. In practice, however, given the 3D nature of the real dynamics, a large enough width is required to guarantee the vertical stability of the structures.

In deriving the stationary speed of structures (equation (15)) we made use of several approximations. The first one is that the tilt angle of the entire structure at impact is always very close to 0. Thus we can assume that the matrix $\mathbb{K}$ is the same for every impact occurring at the same contact point. The vertical relative velocity between the contact point and the vibrating plate has an unspecified value v_y^0 that we assumed to be of the same order of the maximum vertical speed of the plate but it actually fluctuates at each collision. The dashed blue line in figure 2 is obtained as the average between the speeds obtained from equation (15) assuming an equal number of collisions at the front and back leg. We further assume that the vast majority of impacts will be of type III, although four possible collision types are possible (see figure 3).

In order to check the validity of those assumptions we performed direct numerical simulations as illustrated in the flow chart in figure 4. We assume that immediately after collision, the restoring torque on the flexible joint quickly relaxes the structure in its equilibrium configuration. Since only internal forces are involved in this relaxation stage, linear and angular momentum will be conserved so that we can calculate the changes in the linear and angular speeds due to collision directly from $\mathbf{F}^{tot}$:

$$M D v_O = \mathbf{F}^{tot},$$
$$J D \omega = d' \times \mathbf{F}^{tot},$$

where d is $a + 2c$ for collisions at the back leg or $b + 2c$ for collisions at the front leg. A movie showing simulated structures moving on a vibrated plate can be found in the supplementary video.

From simulations, we get that throughout the range of f values, the majority of collisions are of type III followed by a small percentage of type II. The sum of type III and type II collisions account for more then 95% of events. The theoretical prediction in equation (15) has a similar form for collision types III and II and coincide in the limit of $e \to 1$. Therefore, the presence of a small percentage of type II collisions, at low and high f values, will not affect our analytical prediction appreciably.

Experiments were carried out using 3D printed objects consisting of a large rectangular body ($L \times D \times S = 28 \times 8 \times 3$ mm) and two legs of length $\ell = 7.5$ mm (see figure 1). We have considered two families of objects, one with 'thin', flexible legs (thickness $s \simeq 0.5$ mm), one with 'thick' legs (1.0 mm). To further ensure the rigidity condition on the thick legs, a vertical support of 0.5 mm thickness connects the leg tip to the body top. The two contact points are symmetrically displaced from the top centre of mass and their distance is kept fixed at 13 mm while varying the tilt angle f of the legs. For their construction we have used a commercial 3D printer (MakerBot Replicator 2×) and black PLA (Polylactic acid) filament with a vertical step resolution of 0.2 mm. The objects were then placed on a sinusoidally vibrating plexiglas surface and tracked using a feature-tracking algorithm resulting in an estimated error of ± 0.1 mm. As a first step, we measured propulsion speeds by confining their motion along linear tracks having a gap size slightly larger than the object depth D. In figure 2 we report the measured values for the propulsion speed as a function of leg tilt angle f for both flexible and rigid structures. While rigid objects do not show a significant net propulsion, flexible objects run with an average speed that shows a prominent peak at a tilt angle around 10°, in good agreement with theoretical predictions. These measurements were obtained for a vibration frequency set to 90 Hz and a maximum acceleration of 1.8 g corresponding to a maximum plate speed of 32 mm s^{-1}. It is quite remarkable that our structures can run at a top speed of 60 mm s^{-1}, a value that is twice as large as the maximum plate speed, significantly larger than what found for rigid structures [7, 10, 17]. Numerical and theoretical data in figure 2 are evaluated for $e \simeq 0.7$ and $m = 0.1$ which result in the best agreement with experimental curves. By directly observing structures bouncing and sliding on the surface we can

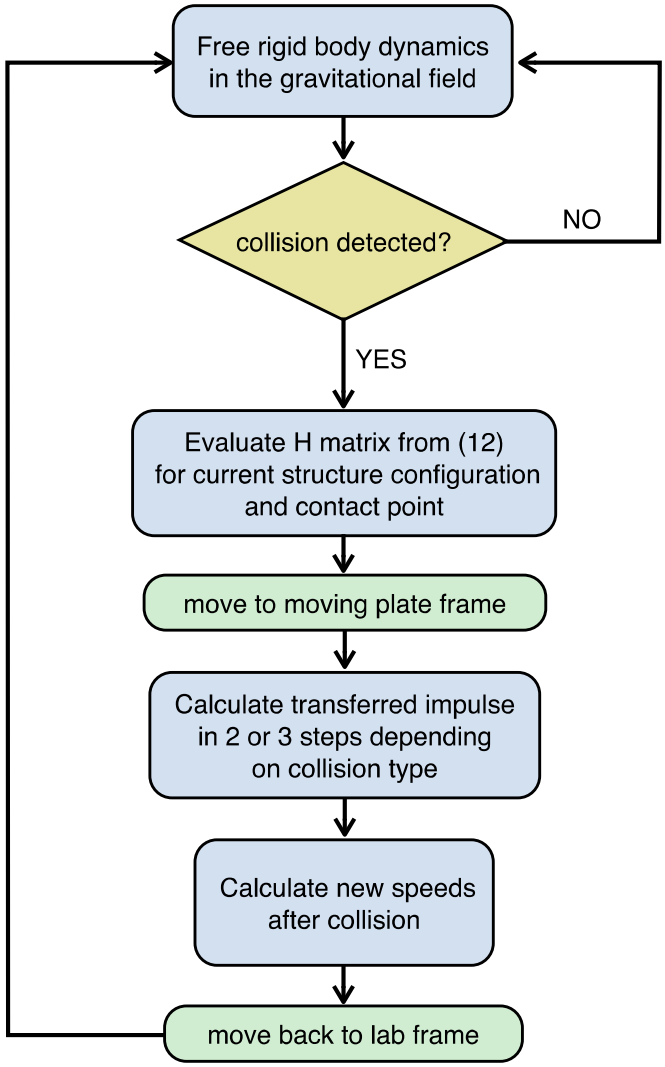

Figure 4. The flowchart of the simulation algorithm.

estimate both the restitution and dynamic friction coefficients and obtain $e = 0.8 \pm 0.1$ and $m = 0.25 \pm 0.02$ which compare well with the best fit values reported above. The measured values for the masses $M = 6.74$ g and $m = 1.034$ g were used in both theory and simulations.

In figure 5 we show a few sample tracks of a $f = 15$ Hz flexible object for increasing values of vibration amplitude at constant frequency. We find a good linear behaviour of the propulsion speed when plotted as a function of the plate speed, showing that the typical relative velocity at impact v_y^0 in our theory is mainly controlled by the plate speed. Finally we study the 2D trajectories traced by our runners moving freely over a planar surface. Figure 6(a) reports the mean squared displacements for three flexible objects with $f = 10$ Hz, 15°, 35° corresponding to high, medium and low propulsion efficiency. The fast and medium runner ($f = 10$ Hz and 15°) are practically always ballistic in the accessible time window, while the slow one displays a transition from a superdiffusive to a diffusive regime at $t \sim 1.0$ s. The diffusivity at longer times is probably due to the 3D nature of the collisions between the legs and the plate, which can occur at random points along the width of the leg and give rise to a fluctuating torque along the vertical direction.

In conclusion, we proposed a theoretical framework that allows to connect the geometrical and dynamical properties of a generic asymmetric object to its propulsion speed when bouncing over a vibrated plate. We found that a large propulsion speed can be generated when using flexible legs and that an optimal tilt angle exists. Using a 3D printer, objects with controllable shapes can be designed leading to different propulsion speeds and also persistent lengths when moving in 2D. This approach could be readily generalized to combine self-propulsion with patches of complex shapes, leading to designable active granulars with shape-controlled steric interactions.

The research leading to these results has received funding from the European Research Council under the European Union's Seventh Framework Programme (FP7/2007-2013)/ERC Grant Agreement No. 307940, as well as from European Union (EU) Horizon 2020 funding, through H2020-MSCA-IF-2014, ActiDoC No. 654688.

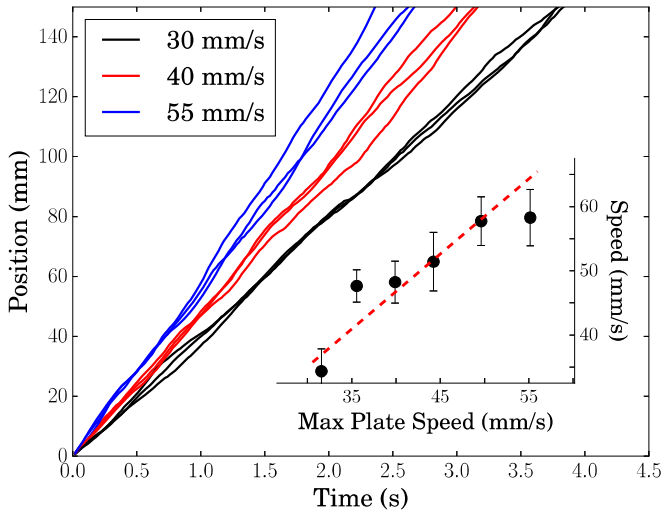

Figure 5. (Main panel) Displacement of the walker (on a single lane track) as a function of time for different values of the maximum plate speed. The object has thin (flexible) legs with tilt angle f = 15 (Inset) Average speed of the walker versus the maximum plate speed (points), the line is a linear fit passing through zero.

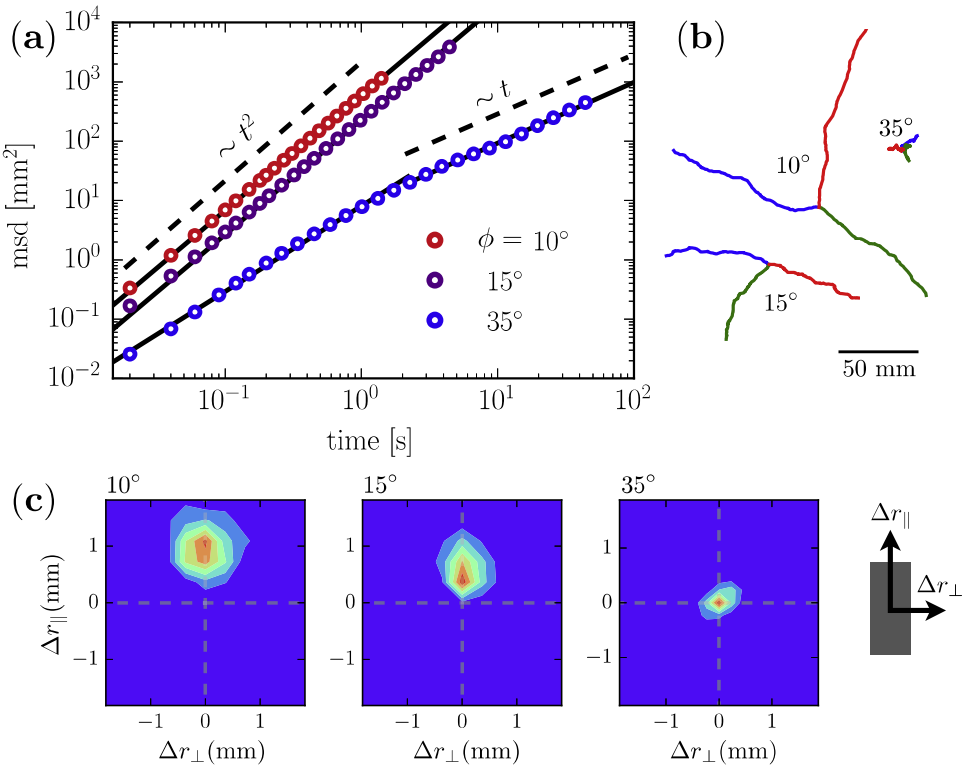

Figure 6. (a) Mean squared displacements from the 2D trajectories. The dashed lines represent ballistic ($\sim t^2$) and diffusive ($\sim t$) behaviour. (b) Sample trajectories for structures with varying leg tilt angle. (c) Probability distributions of parallel and orthogonal displacements (Dt = 40 ms) with respect to the orientation of the structure.

References

[1] Ramaswamy S 2010 *Annu. Rev. Condens. Matter Phys.* **1** 323
[2] Cates M E 2012 *Rep. Prog. Phys.* **75** 042601
[3] Marchetti M C *et al* 2013 *Rev. Mod. Phys.* **85** 1143
[4] Brambilla M, Ferrante E, Birattari M and Dorigo M 2013 *Swarm Intell.* **7** 1
[5] Gnoli A, Petri A, Dalton F, Gradenigo G, Pontuale G, Sarracino A and Puglisi A 2013 *Phys. Rev. Lett.* **110** 120601
[6] Giomi L, Hawley-Weld N and Mahadevan L 2013 *Proc. R. Soc.* A **469** 20120637
[7] Kudrolli A, Lumay G, Volfson D and Tsimring L S 2008 *Phys. Rev. Lett.* **100** 058001
[8] Aranson I S, Volfson D and Tsimring L S 2007 *Phys. Rev.* E **75** 051301

[9] Baskaran A and Marchetti M C 2008 *Phys. Rev.* E **77** 011920
[10] Deseigne J, Dauchot O and Chate H 2010 *Phys. Rev. Lett.* **105** 098001
[11] Deseigne J, Leonard S, Dauchot O and Chate H 2012 *Soft Matter* **8** 5629
[12] Weber C A, Hanke T, Deseigne J, Leonard S, Dauchot O, Frey E and Chate H 2013 *Phys. Rev. Lett.* **110** 208001
[13] Blair D L, Neicu T and Kudrolli A 2003 *Phys. Rev.* E **67** 031303
[14] Volfson D, Kudrolli A and Tsimring L S 2004 *Phys. Rev.* E **70** 051312
[15] Narayan V, Menon N and Ramaswamy S 2006 *J. Stat. Mech.: Theory Exp.* **2006** P01005
[16] Narayan V, Ramaswamy S and Menon N 2007 *Science* **317** 105
[17] Kumar N, Ramaswamy S and Sood A K 2011 *Phys. Rev. Lett.* **106** 118001
[18] Yamada D, Hondou T and Sano M 2003 *Phys. Rev.* E **67** 040301
[19] Dorbolo S, Volfson D, Tsimring L and Kudrolli A 2005 *Phys. Rev. Lett.* **95** 044101
[20] Cicconofri G and DeSimone A 2015 *Int. J. Non-Linear Mech.* **76** 233
[21] Mirtich B and Canny J 1995 Impulse-based simulation of rigid bodies *Proc. of the 1995 Symp. on Interactive 3D graphics* pp 181